Compact Hybrid Cell Based on a Convoluted Nanowire Structure for Harvesting Solar and Mechanical Energy

*Chen Xu and Zhong Lin Wang**

The harvesting of energy from the environment dates back to the age of the windmill and the waterwheel. Their modern counterparts are hydro-power plants, wind farms, solar farms, and more recently, novel piezoelectric devices[1] for power generation from mechanical vibration.[2] Fully utilizing power sources such as light,[3–5] thermal, and mechanical energy is of great importance to our long-term energy needs[6] and sustainable development[7] At a small scale, the development of a wireless self-powered system[8] that harvests its operating energy from the environment is of great importance and an attractive proposition for sensing,[9] personal electronic,[10] and defense technologies. Recently, harvesting multiple type energy using a single device has been a new trend in energy technologies. The first multimode energy harvester[11] has been demonstrated for simultaneously harvesting solar and mechanical energy. Recently, the hybrid cell has been developed for concurrently harvesting biochemical and mechanical energy for in vivo applications.[12,13] This multimode energy harvester has the potential of fully utilizing the energy in the environment under which the devices will be operating.

The prototype of the nanowire-based hybrid cell demonstrated to harvest both solar and mechanical energy is using a dye-sensitized solar cell (DSSC)[14,15] and piezoelectric nanogenerator.[16] However, due to the encapsulation problem posed by the use of the liquid electrolyte[17] in conventional DSSCs, solvent leakage and evaporation are two major obstacles, thus the present hybrid cell is actually a back-to-back physical integration of a nanogenerator and a DSSC on the same substrate, which may limit its performance. We report here an innovative approach that convolutes a solid-state dye-sensitized solar cell[18] and an ultrasonic wave driven piezoelectric nanogenerator into a single compact structure for concurrently harvesting solar and mechanical energy. The structure is fabricated based on vertical ZnO nanowire arrays[19] with the introduction of solid electrolyte and metal coating. Under light illumination of a simulated sun emission (100 mW/cm^2), the optimum power is enhanced by 6% after incorporating the contribution of the nanogenerator. This research provides a platform towards multimode energy harvesting as practical power sources.

The design of the compact hybrid cell (CHC) was to convolute the roles played by the nanowire arrays to simultaneously perform their functionalities in a nanogenerator and a DSSC. The main frame structure consists of two sets of ZnO nanowire arrays that are placed in a "teeth-to-teeth" configuration[20] (**Figure 1**a), as previously demonstrated for the fiber based nanogenerator.[21] The DSSC follows the template offered by the nanowire arrays at the top, which is finally coated with a layer of metal to serve as the electrode for the nanogenerator, and the nanowire array at the bottom acts as piezoelectric structure for converting mechanical energy into electricity. The solar simulator illuminates the device from the top and the ultrasonic wave[16] is applied at the bottom.

To fabricate the solid-state DSSC, the vertically aligned ZnO nanowires (NWs) were grown on an ITO-coated glass substrate (CB-40IN-0107, 4–8 Ω, Delta Technologies, Ltd.) through a hydrothermal method. The substrate was first cleaned by standard acetone/ethanol/IPA/Di water sonication and a thin film of ZnO with 200 nm thickness was deposited by magnetron RF sputter. Then, the ZnO NWs were synthesized by floating the substrate on the nutrient solution surface, which is composed of a 5 mM solution of 1 : 1 ratio $Zn(NO_3)_2$ and hexamethylenetetramine at 80 °C for 24h. After rinsing with acetone, the NWs were immersed in a 0.5 mmol L^{-1} sensitized solution of $(Bu_4N)_2Ru(dcbpyH)_2(NCS)_2$ (N719 dye) in ethanol for 1 h for dye loading. Then the amorphous organic hole-transport material, 2,2′,7,7′-tetrakis(N,N-di-p-methoxyphenylamine) 9,9′-spirobifluorene (OMeTAD), was spun on the dye-sensitized ZnO NWs with 2000 rpm for 60 s and subsequently baked at 100 °C to remove the organic solution. As shown schematically in Figure 1b, a cone-shaped surface was thus created. A continuous gold thin-film coating (60 nm in thickness) resulted in the formation of a cone-shaped electrode as required for the NG described below. Figure 1d shows the scanning electron microscopy (SEM) image of the cone-shaped surface in which the space between the cones was 1–2 μm wide.

For NG fabrication, ZnO NWs (Figure 1c) used for the NG were grown on a GaN (0001) surface using the high-temperature vapor deposition process[22] to achieve uniform polarity. The nanowires were ~2–3 μm in length and the interspacing between the nanowires was 400–700 nm. By stacking the two sets of nanowire arrays interdigitatively face-to-face, the gold-coated cone-shaped electrode on top served as the "zig-zag" electrode[16] for mechanically triggering the nanowires located at the bottom (Figure 1a). This is a functional nanogenerator driven by ultrasonic waves.

The "convolution" of the DSSC and NG in serial order to form a CHC is presented in **Figure 2**a. ITO serves as the cathode while silver (Ag) paste in contact with GaN[23] serves as the anode in this configuration. After connecting to output wires, the entire CHC was sealed and packaged by epoxy resin to prevent infiltration of any liquid except the window of the DSSC.

C. Xu, Prof. Z. L. Wang
School of Materials Science and Engineering
Georgia Institute of Technology
Atlanta, GA 30332, USA
E-mail: zlwang@gatech.edu

DOI: 10.1002/adma.201003696

ADVANCED MATERIALS
www.advmat.de

www.MaterialsViews.com

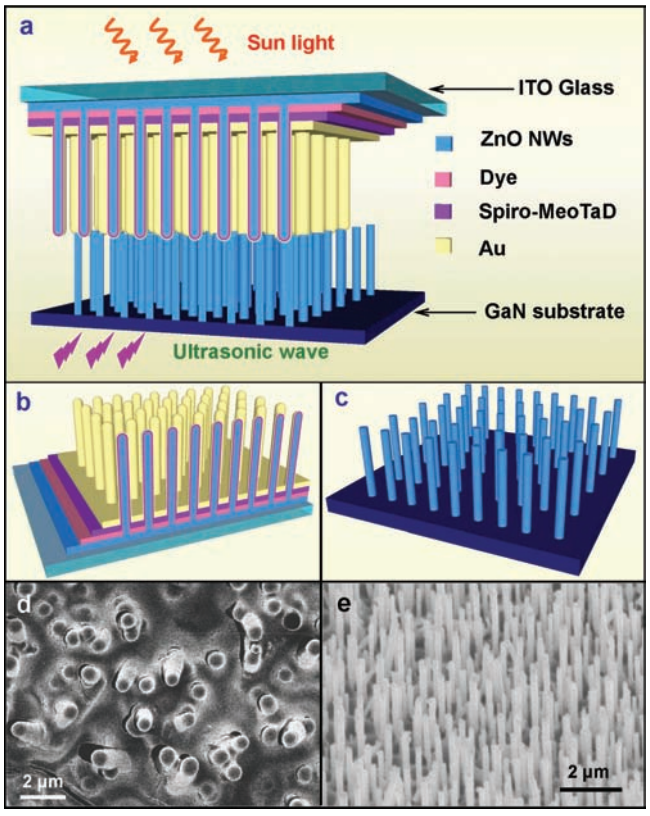

Figure 1. Design of the compact hybrid cell (CHC) structure consisting of a dye-sensitized solar cell (SC) and a nanogenerator (NG). a) Schematic illustration of a CHC, which is illuminated by sunlight from the top and excited by ultrasonic waves from the bottom. The ITO layer on the DSSC part and GaN substrate are defined as the cathode and anode of the CHC, respectively. b) Schematic illustration of a solid state DSSC. c) Schematic illustration of a vertically aligned ZnO nanowire array grown on a GaN substrate. d) Top view SEM image of the DSSC. e) SEM image of the as-grown ZnO nanowire array using the high-temperature vapor deposition method for fabricating the NG.

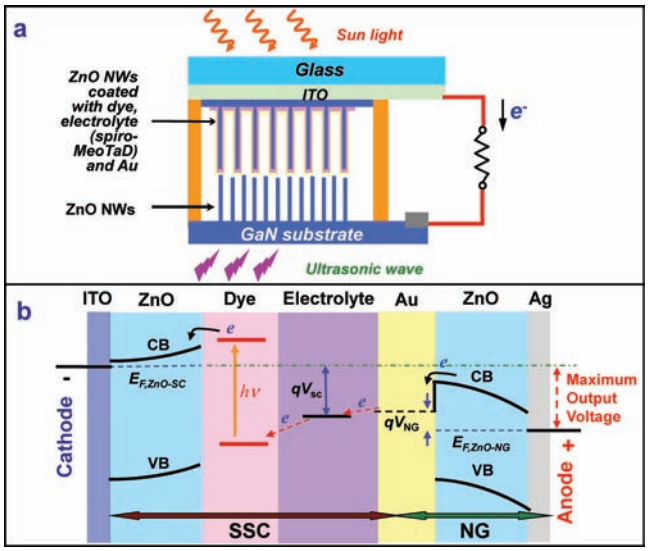

Figure 2. Design and physical principle of the CHC. A) Schematic structure of a CHC. B) Electron energy band diagram of the CHC, showing that the maximum output voltage is a sum of those produced by the DSSC and NG. The abbreviations are: conduction band (CB), valence band (VB), and Fermi level (E_F).

The working principle of the CHC is presented by the electron energy band diagram (Figure 2b). The electrons were promoted through the two devices consecutively by the piezoelectric and photovoltaic potential.[11] The maximum achievable output voltage is the difference between the Fermi level of the ZnO NWs in the DSSC ($E_{F,\ ZnO\text{-}SC}$) and that of the ZnO NWs in the NG ($E_{F,\ ZnO\text{-}NG}$). It is a summation of the output voltages of the NG and DSSC. In the NG section, the gap between the Fermi level of the ZnO NWs ($E_{F,\ ZnO\text{-}NG}$) and that of the gold determined the maximum voltage output of the NG (V_{NG}). The Au–ZnO junction forms a Schottky contact[24] because Au has a work function of 4.8 eV that is greater than the electron affinity of ZnO (4.5eV), which serves as a "gate" that blocks the back flow of electrons. When the gold electrode slowly pushed a NW like an AFM tip,[1] a strain field was created across the NW width, with the outer surface in tensile strain and the inner surface in compressive strain. The piezoelectric potential at the compressive side of the nanowire sets the Schottky contact as forward biased and drives the electrons to across the Au–ZnO junction.[20] Through an electron-transfer process,[25] these charge carriers continue transport in the solid state electrolyte into the DSSC[18] In the DSSC section of Figure 2b, the maximum voltage output (V_{SC}) is dictated by the difference between the ZnO's Fermi level ($E_{F,\ ZnO\text{-}SC}$) and the electrochemical potential of the electrolyte. Visible-light absorption by the dye sensitizer excites electron transfer to the conduction band of ZnO. The electron injection from the excited sensitizer into ZnO is followed by regeneration of the dye sensitizer by the electron from OMeTAD. The electrons in the conduction-band of ZnO and the holes in the electrolyte are separated and subsequently transported to the contact electrodes.

Both DSSC and NG units of the CHC can work independently and conjunctionally. The CHC was characterized by affixing it on the water surface in an ultrasonic generator cavity with the transparent DSSC side facing the sunlight source and the NG side in direct contact with the water underneath,[26] where an ultrasonic generator with a frequency of ~41 kHz was applied from the bottom side (Figure 1a). *J–V* curves were recorded for the CHC, DSSC, and NG, respectively. The short-circuit current was measured by serially connecting the CHC to a DS345 30MHz synthesized function generator (Stanford Research Systems) with a resistance of 50 Ω sweeping from –1 to +1 V as external load. The current signal was using a DL 1211 preamplifier (DL instruments). All of the signals were converted through a BNC-2120 analog-to-digital converter (National Instruments) and recorded by a computer. The photovoltaic performance of the DSSC for CHC was first characterized under simulated sunlight illumination (AM 1.5G simulated sun light 300 W model 91160, Newport) without applying ultrasonic waves. The open-circuit voltage (U_{OC}–SC) was 0.42 V and the short-circuit current density (J_{SC}–SC) was 0.25 mA cm^{-2} (**Figure 3**a). The fill factor of the DSSC reached 30.6% corresponding to an overall energy conversion efficiency of 0.03%,

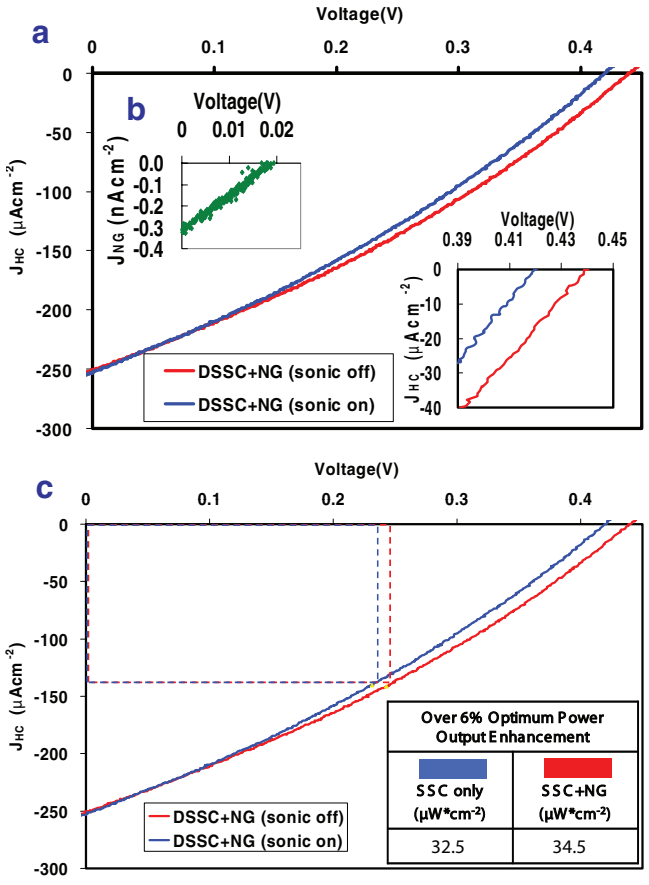

Figure 3. Performance of the CHC. A) A comparison of *J–V* characteristics of a CHC when illuminated by simulated sunlight with (red curve) and without (blue curve) turning on the ultrasonic wave excitation. Inset is an expanded output of the open circuit voltage U_{OC} points around the axial cross point, showing the increment of U_{OC} for ~19 mV after turning on ultrasonic waves. B) *J–V* characteristic of the NG when subjected to the ultrasonic wave's excitation, but without sunlight illumination. C) A comparison in power output *J–V* characteristics of a CHC. The rectangle area is the optimal power output for the CHC.

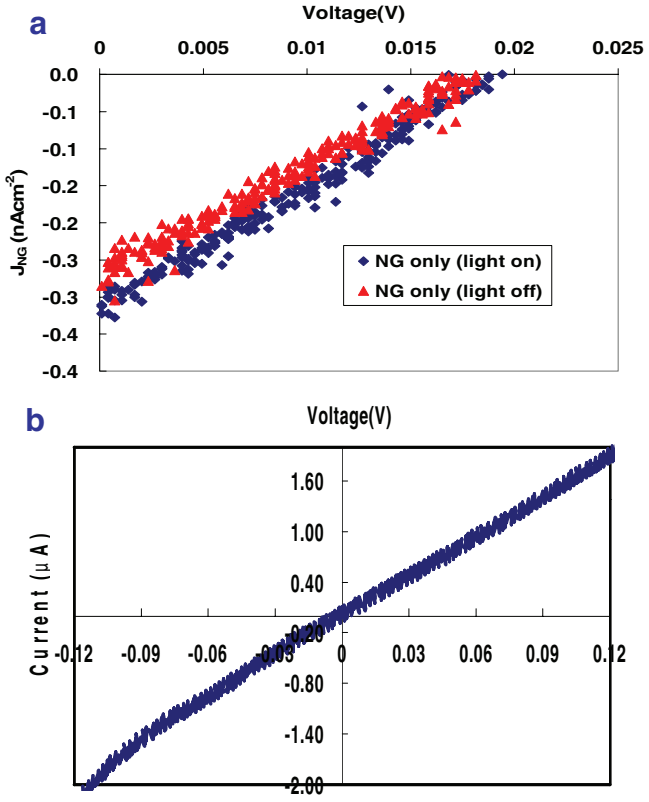

Figure 4. Performance of piezoelectric nanogenerator. A) *J–V* characteristic of the NG, without including the DSSC unit in the measurement circuit, when excited by ultrasonic waves with (red curve) and without (blue curve) turning on simulated sunlight. It shows almost no change in U_{OC} of the NG even when the simulated sunlight was turned on or off. B) *I–V* curve recorded from the NG part of the hybrid cell at near-zero-point region when both the sunlight and ultrasonic wave were off. The *I–V* curve came right across the zero point, showing no contribution from the DSSC to the NG when the hybrid cell was measured in dark. These tests are essential to exclude the influence of DSSC to the characterization of NG.

which is comparable to that of the ZnO based solid state DSSC.[27]

The NG was characterized by introducing ultrasonic waves through the water media without sunlight illumination; the corresponding *J–V* curve showed that the U_{OC}–NG was ~0.019 V and the I_{NG} was ~0.3 pA cm^{-2} (the left inset of Figure 3a). A *J–V* curve of the NG (**Figure 4**a) was recorded when the sunlight was turned on and off. The corresponding Uoc-NG showed no change, indicating that there was no contribution from the SC to the NG when only NG was being characterized. Furthermore, An *I–V* curve of the NG was also recorded at near-zero-point region when the device was in dark condition without applying ultrasonic waves. As shown in Figure 4b, the curve passed right across the zero point. The data prove that the DSSC and NG units in the CHC can work independently when only one type of energy source is available. ZnO based solid state DSSC was purposely chosen because the output of the DSSC is comparable to that of NG. But it can be largely improved by using TiO_2 based solid state DSSC.

To demonstrate the technological feasibility of the CHC for simultaneous harvesting of solar and mechanical energy, we measured the *J–V* curve on CHC under different condition. When the full sunlight source was on and the ultrasonic wave source was off, the CHC exhibited a U_{OC} of 0.415 V and J_{SC} of 252 μAcm^{-2} (blue curve in Figure 3a). When both the ultrasonic wave and sunlight were turned on, the U_{OC} reached 0.433 V, while the J_{SC} remained at 252 μAcm^{-2} (red curve in Figure 3a). The output voltage of the CHC showed a 19 mV difference when turning on and off the ultrasonic wave, as shown by the expanded plot of U_{OC} in the right-hand inset of Figure 3a, which is just the output voltage of the NG when the sunlight was off (Figure 3b).

The main advantage of this new CHC is that, unlike our previous hybrid cell,[11] the new CHC is a solid state device without liquid electrolyte and two parts are convolutedly designed in a single compact. In particular, the possibility of solvent leakage and evaporation from DSSC is no longer an issue. Moreover, the single compact design makes it truly single device that has the ability to harvest both solar and mechanical energy.

ADVANCED MATERIALS
www.advmat.de

www.MaterialsViews.com

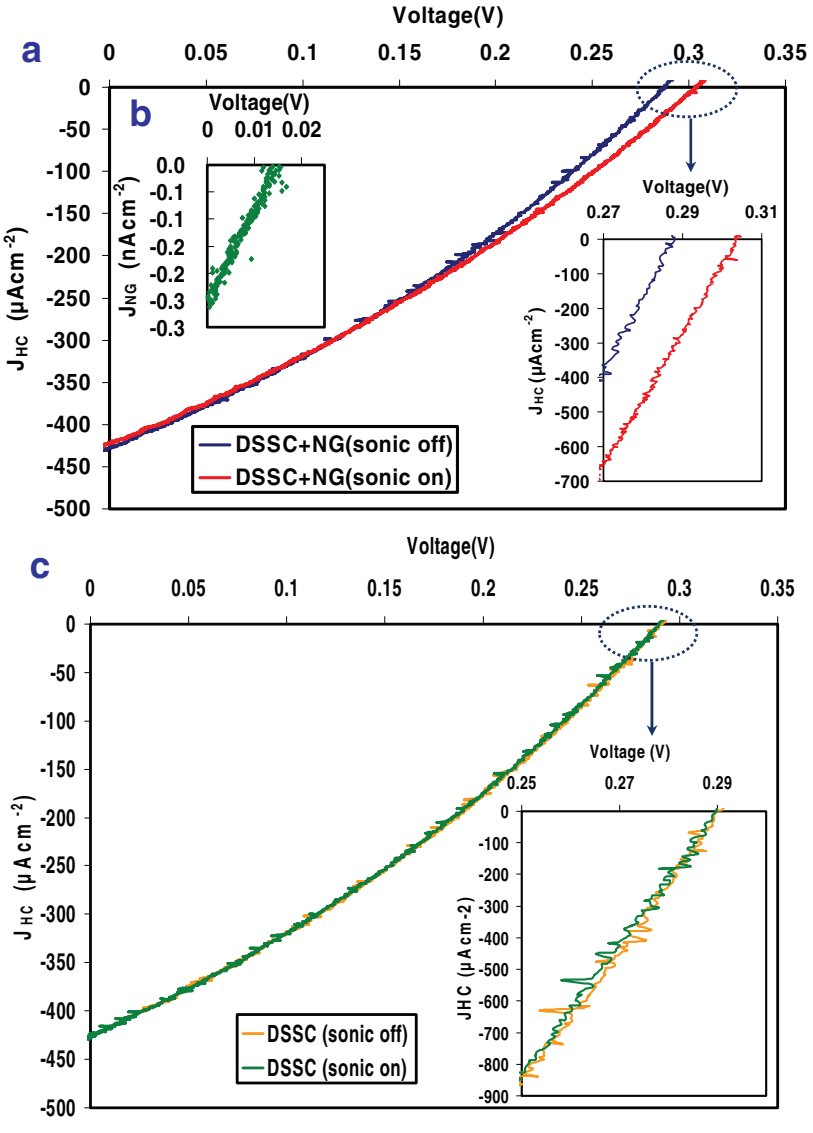

Figure 5. Controlled performance of the CHC. A) *J–V* characteristics of another CHC when a simulated sunlight was illuminating onto the SC side and the ultrasonic wave was turned on (red curve) and off (blue curve). B) *J–V* characteristic of the NG component when subjected to ultrasonic wave excitation but with sunlight off. C) *J–V* characteristic of the DSSC, without including the NG unit in the measurement circuit, when illuminated by a simulated sunlight with (green curve) and without (orange curve) turning on ultrasonic waves. Inset is an expanded plot around the U_{OC} points, showing there is almost no change in U_{OC} by turning on ultrasonic waves. The open circuit voltage U_{OC} point was not affected by the ultrasonic wave, simply ruling out the contribution from the fluctuation in NG resistance to the performance of the SC.

In order to further confirm that the increase of U_{OC} is truly coming from the NG unit, another set of *J–V* characteristic was measured between the cathode and anode of DSSC unit without including the NG unit in the measurement circuit. The performance of the CHC was shown in the *J–V* curves (**Figure 5**a) with the NG performance in Figure 5b. By turning on and off the ultrasonic waves, the *J–V* curves exhibited almost an identical trace (Figure 5c). Particularly, the U_{OC}-SC remained at the same point, as shown by the expanded plot of U_{OC} in the inset of Figure 5c.

To visually see the optimum power output from the *J–V* curve, the product of current density and voltage was calculated. The area of the rectangle was representing the optimum output power density. By comparing the area difference, we can tell that the CHC shows an enhanced energy harvesting performance in comparison to the performance of either one of the devices. When only the DSSC component was in operation and under the one full sunlight illumination as (Figure 3c), the optimum output power density (blue rectangle) was found to be 32.5 μW cm^{-2} at J_{SC} = 140 μAcm^{-2} and U_{OC} = 0.231 V. When both DSSC and NG were simultaneously operating in serial connection, the corresponding output power density was 34.5 μWcm^{-2} at J_{SC} = 141 μA cm^{-2} and U_{OC} = 0.243 V (red rectangle). An increment (ΔP_{HC}) of 2 μW cm^{-2} in power density was thus achieved after turning the ultrasonic wave on, which was over 6% enhancement in optimum power. Therefore, in addition to the open circuit voltage, the CHC successfully added up the total power outputs from both SC and NG.

In summary, we have developed a fully integrated solid-state compact hybrid cell that comprises "convoluted" ZnO nanowire structures for concurrently harvesting both solar and mechanical energy using a single device. The compact hybrid cell is based on a conjunction design of the organic solid-state DSSC and piezoelectric nanogenerator in one compact structure; it not only shows an increase in the output voltage but also in the output power as the driving ultrasonic wave is turned on, clearly demonstrating its potential for simultaneously harvesting multiple types of energy. An increase of 6% in optimum power for the CHC was demonstrated by incorporating the contribution of the nanogenerator. Therefore, the CHC is more efficient for fully utilizing the available solar and mechanical energy in our living environment for powering small electronic devices for independent, sustainable, and mobile operation.

Acknowledgements

Research was supported by DARPA (HR0011 – 09-C-0142, Program manager, Dr. Daniel Wattendorf), Airforce, BES DOE (DE-FG02 – 07ER46394), NSF (DMS0706436, CMMI 0403671), National Institute For Materials, Japan (Agreement DTD 1 Jul. 2008), and US Airforce. Z.L.W thanks the support from the WCU program administrated by UNIST, Korea.

Received: October 8, 2010
Published online: January 7, 2011

[1] Z. L. Wang, J. H. Song, *Science* **2006**, *312*, 242.
[2] Z. L. Wang, *Sci. Am.* **2008**, *298*, 82.
[3] B. Z. Tian, X. L. Zheng, T. J. Kempa, Y. Fang, N. F. Yu, G. H. Yu, J. L. Huang, C. M. Lieber, *Nature* **2007**, *449*, 885.
[4] W. G. Pfann, W. Vanroosbroeck, *J. Appl. Phys.* **1954**, *25*, 1422.
[5] W. U. Huynh, J. J. Dittmer, A. P. Alivisatos, *Science* **2002**, *295*, 2425.
[6] M. S. Dresselhaus, G. W. Crabtree, M. V. Buchanan, *MRS Bull.* **2005**, *30*, 518.
[7] M. S. Dresselhaus, I. L. Thomas, *Nature* **2001**, *414*, 332.
[8] S. Xu, Y. Qin, C. Xu, Y. G. Wei, R. S. Yang, Z. L. Wang, *Nat. Nanotechnol.* **2010**, *5*, 366.
[9] Y. Cui, C. M. Lieber, *Science* **2001**, *291*, 851.
[10] J. A. Paradiso, T. Starner, *IEEE Perv. Comp.* **2005**, *4*, 18.
[11] C. Xu, X. D. Wang, Z. L. Wang, *J. Am. Chem. Soc.* **2009**, *131*, 5866.
[12] F. Patolsky, B. P. Timko, G. F. Zheng, C. M. Lieber, *MRS Bull.* **2007**, *32*, 142.
[13] B. J. Hansen, Y. Liu, R. S. Yang, Z. L. Wang, *ACS Nano* **2010**, 4, 3647.
[14] B. Oregan, M. Gratzel, *Nature* **1991**, *353*, 737.
[15] M. Law, L. E. Greene, J. C. Johnson, R. Saykally, P. D. Yang, *Nat. Mater.* **2005**, *4*, 455.
[16] X. D. Wang, J. H. Song, J. Liu, Z. L. Wang, *Science* **2007**, *316*, 102.
[17] M. K. Nazeeruddin, A. Kay, I. Rodicio, R. Humphrybaker, E. Muller, P. Liska, N. Vlachopoulos, M. Gratzel, *J. Am. Chem. Soc.* **1993**, *115*, 6382.
[18] U. Bach, D. Lupo, P. Comte, J. E. Moser, F. Weissortel, J. Salbeck, H. Spreitzer, M. Gratzel, *Nature* **1998**, *395*, 583.
[19] L. E. Greene, M. Law, J. Goldberger, F. Kim, J. C. Johnson, Y. F. Zhang, R. J. Saykally, P. D. Yang, *Angew. Chem. Int. Ed.* **2003**, *42*, 3031.
[20] S. Xu, Y. G. Wei, J. Liu, R. Yang, Z. L. Wang, *Nano Lett.* **2008**, *8*, 4027.
[21] Y. Qin, X. Wang, Z. L. Wang, *Nature* **2009**, *457*, 340.
[22] X. D. Wang, J. H. Song, P. Li, J. H. Ryou, R. D. Dupuis, C. J. Summers, Z. L. Wang, *J. Am. Chem. Soc.* **2005**, *127*, 7920.
[23] X. D. Wang, J. H. Song, C. J. Summers, J. H. Ryou, P. Li, R. D. Dupuis, Z. L. Wang, *J. Phys. Chem. B* **2006**, *110*, 7720.
[24] J. Liu, P. Fei, J. H. Song, X. D. Wang, C. S. Lao, R. Tummala, Z. L. Wang, *Nano Lett.* **2008**, *8*, 328.
[25] J. Kruger, R. Plass, M. Gratzel, P. J. Cameron, L. M. Peter, *J. Phys. Chem. B* **2003**, *107*, 7536.
[26] J. Liu, P. Fei, J. Zhou, R. Tummala, Z. L. Wang, *Appl. Phys. Lett.* **2008**, *92*.
[27] M. Boucharef, C. Di Bin, M. S. Boumaza, M. Colas, H. J. Snaith, B. Ratier, J. Boucle, *Nanotechnology* **2010**, *21*.